MULTI-SCALE OVERLAPPING DOMAIN DECOMPOSITION TO CONSIDER LOCAL EFFECTS IN THE ANALYSIS OF PIPES

R. Emre Erkmen[1,*], Ashkan Afnani[1]
[1] School of Civil and Environmental Engineering, University of Technology, Sydney, Broadway, NSW 2007, Sydney, Australia.*Email: emre.erkmen@uts.edu.au

ABSTRACT

Elevated pipelines are commonly encountered in petro-chemical and industrial applications. Within these applications, pipelines normally span hundreds of meters and are thus analysed using beam-type one-dimensional finite elements when the global behaviour of the pipeline is sought at a reasonably low computational cost. Standard beam-type elements, while computationally economic, are based on the assumption of rigid cross-section. Thus, they are unable to capture the effects of cross-sectional localized deformations. Such effects can be captured through shell-type finite element models. For long pipelines, shell models become prohibitively expensive. Within this context, the present study formulates an efficient numerical modelling technique which effectively combines the efficiency of beam-type solutions while retaining the accuracy of shell-type solutions. An appealing feature of the model is that it is able to split the global analysis based on simple beam-type elements from the local analysis based on shell-type elements. This is achieved through a domain-decomposition procedure within the framework of the bridging multi-scale method of analysis. Solutions based on the present model are compared to those based on full shell-type analysis. The comparison demonstrates the accuracy and efficiency of the proposed method.

KEYWORDS

Finite element method, Multiscale Method, pipe, local buckling

INTRODUCTION

Thin-walled pipes are widely used in industrial applications. Usually, they are susceptible to buckling, and it is important to predict their nonlinear response accurately. Pipes usually span much larger distances in comparison to their cross-sectional dimensions. As such, beam-type elements are commonly adopted in their analysis. Standard beam-type elements, however, are based on the assumption of rigid cross-section and thus, cannot consider the deformations of the cross-section such as local buckling (Karamanos, 2002) and only allow considerations of the global behaviour such as flexural-buckling (Hobbs, 1981). In contrast, Shell-type finite elements can capture local effects. The buckling response for long pipes under combinations of bending, axial force, and external pressure using shell analyses were investigated in (Houliara & Karamanos, 2006, 2010; Karamanos & Tassoulas, 1996). On the other hand, shell elements are computationally more expensive and time-consuming, and for typical pipeline networks spanning hundreds of meters, such shell analyses become impractical.

Research on computational mechanics has been increasingly focusing on adaptive numerical analysis strategies such as mesh-free methods e.g. (Belytschko et al., 1996; E. Erkmen & Bradford, 2011), Generalized-FEM (Babuška & Melenk, 1997; Belytschko et al., 2001) and Multi-scale methods (Hughes & Sangalli, 2007; Liu et al., 2000), which improve the efficiency and accuracy of the numerical results by refining the model only where required and without changing the global simpler model of the whole structure. Common to these numerical methods is that the partition of unity concept is exploited to allow overlapping decompositions of the analysis domain so that a local enrichment can be seamlessly incorporated (Babuška et al., 2003; Li & Liu, 2002). In which naturally give rise to multiple scales in the deformation fields, such as crack propagation e.g. (Haidar et al., 2003; Mosler, 2005), or localized damage problems e.g. (Mosler, 2005) multi-scale numerical analysis techniques have been effectively used. In particular, the Bridging multi-scale method, which was originally developed to enrich the nodal values of the FEM solution with mesh-free solution (Liu et al., 1997), provides a basis to couple problems based on two different physical assumptions. The appealing feature of the Bridging

multi-scale method is that it can split the global analysis, which is based on simplified assumptions, from the local analysis which requires more sophisticated modelling. Bridging multi-scale method was previously used to incorporate nano-mechanics and atomistic behaviour into the local model e.g. (Liu et al., 2006; Qian et al., 2004; Wagner & Liu, 2003).

In pipe buckling behaviour, the interaction of local with global modes also gives rise to multiple scales in the deformation fields. In order to capture the effect of local deformations, shell formulations have been utilised in the past e.g. (Ju & Kyriakides, 1992; Ozkan & Mohareb, 2009; Song & Tassoulas, 1993; Weicker et al., 2010). Localized plasticity effects have also been incorporated into pipeline analysis through generalized plasticity models (Nowzartash & Mohareb, 2004). In order to capture ovalization in pipe elbows, efficient beam type formulations were developed in (Bathe & Almeida, 1982; Militello & Huespe, 1988). Recently, R. E. Erkmen (2013) developed an analysis procedure based on the Bridging multi-scale method of Liu et al. (2006), in order to incorporate local deformation effects in the analysis of thin-walled members. This approach allows employment of two kinematic models within the numerical analysis, and while simple beam-type elements are used for the analysis of the overall structure, more sophisticated shell-type elements are employed for the local fine-scale analysis in a relatively narrow span of the member. In the present study, we extend the procedure developed in R. E. Erkmen (2013) for the elasto-plastic analysis of pipes. Comparisons with full shell- and beam-type models are provided in order to illustrate the efficiency of the proposed analysis.

BEAM-TYPE ANALYSIS

A beam formulation based on the classical kinematic assumptions of the Euler-Bernoulli beam theory is used for the global analysis. The beam element strain vector can be written in terms of linear and second order nonlinear terms, i.e. $\bar{\boldsymbol{\varepsilon}}=\bar{\boldsymbol{\varepsilon}}_L+\bar{\boldsymbol{\varepsilon}}_N$. Orientation of the displacement components of the beam element are shown in Figure 1.

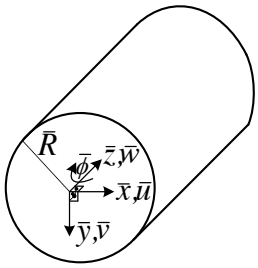

Figure 1 Deflections of the beam formulation

The linear axial and shear strains $\bar{\varepsilon}_L$ and $\bar{\gamma}_L$ can be obtained in terms of the derivatives of displacements $\bar{u},\bar{v},\bar{w}$ and the angle of twist $\bar{\phi}$ as

$$\bar{\boldsymbol{\varepsilon}}_L=\langle \bar{\varepsilon}_L \quad 0 \quad \bar{\gamma}_L \quad 0\rangle^{\mathrm{T}}=\bar{\mathbf{S}}\bar{\boldsymbol{\chi}}_L \tag{1}$$

where $\bar{\mathbf{S}}$ and $\bar{\boldsymbol{\chi}}_L$ are given explicitly as

$$\bar{\boldsymbol{\varepsilon}}_L=\langle \bar{\varepsilon}_L \quad 0 \quad \bar{\gamma}_L \quad 0\rangle^{\mathrm{T}}=\bar{\mathbf{S}}\bar{\boldsymbol{\chi}}_L \tag{2}$$

$$\bar{\boldsymbol{\chi}}_L{}^{\mathrm{T}}=\langle \bar{w}' \quad \bar{u}'' \quad \bar{v}'' \quad \bar{\phi}'\rangle \tag{3}$$

In Eq. 2 , $\bar{x}$ and $\bar{y}$ identify coordinates of a point on the cross-section, and $\bar{R}$ is the radius of the pipe. The nonlinear strains can be written as

$$\bar{\boldsymbol{\varepsilon}}_N=\langle \bar{\varepsilon}_N \quad 0 \quad \bar{\gamma}_N \quad 0\rangle^{\mathrm{T}}=\bar{\mathbf{S}}\bar{\boldsymbol{\chi}}_N \tag{4}$$

in which $\bar{\varepsilon}_N$ is the nonlinear axial strain and $\bar{\gamma}_N$ is considered to vanish. The vector of second-order displacement derivatives $\bar{\boldsymbol{\chi}}_N$ in Eq. 4 is given as

$$\bar{\boldsymbol{\chi}}_N{}^{\mathrm{T}} = \left\langle \frac{1}{2}\left(\bar{u}'^2 + \bar{v}'^2\right) \quad 0 \quad 0 \quad 0 \quad 0 \right\rangle \tag{5}$$

The element is developed by using linear interpolations for $\bar{w}$ and $\bar{\phi}$ and cubic interpolations for $\bar{u}$ and $\bar{v}$. Consequently, the equilibrium equations for static analysis can be obtained in the variational form as

$$\delta\bar{\Pi} = \int_L \int_A \delta\bar{\boldsymbol{\varepsilon}}^{\mathrm{T}} \bar{\boldsymbol{\sigma}} \mathrm{d}A\,\mathrm{d}\bar{z} - \delta\bar{\mathbf{d}}^{\mathbf{T}}\bar{\mathbf{f}} = 0 \tag{6}$$

in which A is the cross-sectional area, L is the beam span and $\bar{\mathbf{f}}$ is the external load vector. In this study, in the regions where no local deformations occur, the material behaviour is assumed elastic. Thus, in Eq. 6, the beam stresses can be obtained directly from the strains using the linear stress-strain relationship for an isotropic material. The first variation of the strain vector can be written as

$$\delta\bar{\boldsymbol{\varepsilon}} = \bar{\mathbf{S}}\bar{\mathbf{B}}\delta\bar{\mathbf{d}} \tag{7}$$

The incremental equilibrium equations can be obtained by subtracting the virtual work expressions at two neighbouring equilibrium states and then linearising the result by omitting the second- and higher-order terms, i.e.,

$$\Delta\left(\delta\bar{\Pi}\right) \approx \delta\bar{\mathbf{d}}^{\mathbf{T}}\bar{\mathbf{K}}\Delta\bar{\mathbf{d}} - \delta\bar{\mathbf{d}}^{\mathbf{T}}\Delta\bar{\mathbf{f}} = 0 \tag{8}$$

where $\bar{\mathbf{K}}$ is the stiffness matrix of the global beam model, i.e.,

$$\bar{\mathbf{K}} = \int_L \int_A \bar{\mathbf{B}}^{\mathrm{T}}\bar{\mathbf{S}}^{\mathrm{T}}\bar{\mathbf{E}}\bar{\mathbf{S}}\bar{\mathbf{B}}\mathrm{d}A\mathrm{d}\bar{z} + \int_L \bar{\mathbf{M}}_\sigma \mathrm{d}\bar{z} \tag{9}$$

in which $\bar{\mathbf{M}}_\sigma \Delta\bar{\mathbf{d}} = \delta\bar{\mathbf{B}}^{\mathrm{T}} \int_A \bar{\mathbf{S}}^{\mathrm{T}}\bar{\boldsymbol{\sigma}}\mathrm{d}A$.

SHELL-TYPE ANALYSIS

Strains of the shell-type analysis are composed of linear strains due to (a) membrane deformation $\hat{\boldsymbol{\varepsilon}}_{mm}$, (b) plate bending deformations $\hat{\boldsymbol{\varepsilon}}_b$, and (c) nonlinear components of strains due to membrane and plate bending action $\hat{\boldsymbol{\varepsilon}}_N$, i.e.,

$$\hat{\boldsymbol{\varepsilon}} = \hat{\boldsymbol{\varepsilon}}_{mm} + \hat{\boldsymbol{\varepsilon}}_b + \hat{\boldsymbol{\varepsilon}}_N = \left\langle \hat{\varepsilon}_x \quad \hat{\varepsilon}_y \quad \hat{\gamma}_{xy} \quad \hat{\gamma}_m \right\rangle^{\mathrm{T}} \tag{10}$$

Figure 2 shows the x and y axes defining a plane tangential to the mid-surface of the shell and z-axis is normal to the mid-surface.

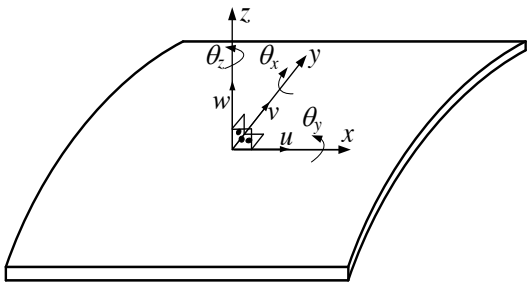

Figure 2 Local deflections of the shell element

The vector of linear components for the membrane strain $\hat{\boldsymbol{\varepsilon}}_{mm}$ can be written as

$$\hat{\boldsymbol{\varepsilon}}_{mm}^{T} = \left\langle \hat{\boldsymbol{\varepsilon}}_m{}^{T} \;\middle|\; \frac{1}{2}\left(\frac{\partial\hat{v}_0}{\partial x} - \frac{\partial\hat{u}_0}{\partial y}\right) - \hat{\theta}_z \right\rangle = \left\langle \frac{\partial\hat{u}_0}{\partial x} \quad \frac{\partial\hat{v}_0}{\partial y} + \frac{\partial f}{\partial r}\hat{\theta}_y \quad \frac{\partial\hat{u}_0}{\partial y} + \frac{\partial\hat{v}_0}{\partial x} \;\middle|\; \frac{1}{2}\left(\frac{\partial\hat{v}_0}{\partial x} - \frac{\partial\hat{u}_0}{\partial y}\right) - \hat{\theta}_z \right\rangle \tag{11}$$

in which $\hat{\theta}_x$ and $\hat{\theta}_y$ are rotations in local *x*-*z* and *y*-*z* planes respectively, $\hat{\theta}_z$ is the drilling rotation about the *z* axis, and $\hat{u}_0$ and $\hat{v}_0$ are the displacements of the mid-surface in the local *x*-*y* plane (Figure 2). In Eq. 11 the term $\left(\partial f/\partial r\right)\hat{\theta}_y$ is added according to Marguerre shallow shell theory (Robert D. Cook, 1990). As shown in Figure 3, $f = f\left(r\right)$ is the expression for the elevation of the arch in *Z*-*Y* plane in terms of coordinate *r*.

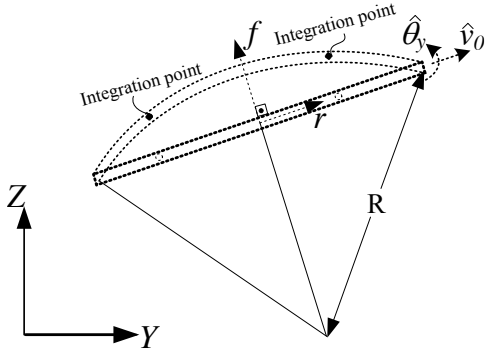

Figure 3 Arch elevation used in shell formulation

In calculating the element length and locations of the integration points, the arch length was considered. For the membrane component of the shell-type element, the finite element of Ibrahimbegovic et al. (1990) employing drilling degrees of freedom is adopted herein, so that non-coplanar elements can be easily assembled. According to Mindlin-Reissner theory (R.D. Cook et al., 2002), the plate bending strains can be written as

$$\hat{\boldsymbol{\varepsilon}}_b = -z\left\langle \hat{\boldsymbol{\chi}} \;\vdots\; 0 \right\rangle^T = -z\left\langle \frac{\partial \hat{\theta}_x}{\partial x} \quad \frac{\partial \hat{\theta}_y}{\partial y} \quad \frac{\partial \hat{\theta}_x}{\partial y}+\frac{\partial \hat{\theta}_y}{\partial x} \;\vdots\; 0 \right\rangle^T \tag{12}$$

in which $\hat{\boldsymbol{\chi}}$ is the curvature vector. It is assumed that the second order longitudinal displacement derivatives, second order lateral strains and second order shear strains are negligibly small. Thus, the nonlinear strain component can be written as

$$\hat{\boldsymbol{\varepsilon}}_N \approx \left\langle \frac{1}{2}\left(\frac{\partial \hat{w}_0}{\partial x}\right)^2+\frac{1}{2}\left(\frac{\partial \hat{v}_0}{\partial x}\right)^2 \quad 0 \quad 0 \;\vdots\; 0 \right\rangle^T \tag{13}$$

in which $\hat{w}_0$ is the out of plane deflection of the mid-surface in local z direction (Figure 2). The shell analysis is elasto-plastic, and for convenience, we apply the one step forward Euler numerical procedure as described in (Crisfield, 1991). Under plane stress plasticity conditions, i.e. $\hat{\sigma}_z = \hat{\tau}_{yz} = \hat{\tau}_{zx} = 0$, the von Mises yield criterion is used to determine whether the trial stresses are elastic. According to the forward Euler procedure in (Crisfield, 1991) since $\varepsilon_z \neq 0$, a four-dimensional yield surface is assumed. The plastic strain increment is obtained by using Prandtl-Reuss flow rule for associative plasticity. The equilibrium equation of the shell analysis can be obtained in the variational form as

$$\delta\hat{\Pi} = \int_L \int_A \delta\hat{\boldsymbol{\varepsilon}}^{\mathrm{T}} \hat{\boldsymbol{\sigma}} \mathrm{d}A\mathrm{d}z - \delta\hat{\mathbf{d}}^{\mathrm{T}}\,\hat{\mathbf{f}} = 0 \tag{14}$$

It should be noted that the virtual work functional of the shell element is modified in order to avoid numerical stability issues with Allman type interpolations of the membrane component (Ibrahimbegovic et al., 1990). Similar to the beam analysis, the variation of the strain tensor can be written as

$$\delta\hat{\boldsymbol{\varepsilon}} = \hat{\mathbf{S}}\hat{\mathbf{B}}\delta\hat{\mathbf{d}} \tag{15}$$

Similar to the beam formulation, the incremental equilibrium equations for the shell formulation can be obtained as

$$\Delta\left(\delta\hat{\Pi}\right) \approx \delta\hat{\mathbf{d}}^{\mathbf{T}}\hat{\mathbf{K}}\Delta\hat{\mathbf{d}} - \delta\hat{\mathbf{d}}^{\mathbf{T}}\Delta\hat{\mathbf{f}} = 0 \tag{16}$$

where $\hat{\mathbf{K}}$ is the tangent stiffness matrix of the shell model, i.e.,

$$\hat{\mathbf{K}}=\int_L\int_A \hat{\mathbf{B}}^{\mathrm{T}}\hat{\mathbf{S}}^{\mathrm{T}}\hat{\mathbf{E}}_{ep}\hat{\mathbf{S}}\hat{\mathbf{B}}\mathrm{d}A\mathrm{d}\bar{z}+\int_L \hat{\mathbf{M}}_{\sigma}\,\mathrm{d}\bar{z} \tag{17}$$

where $\hat{\mathbf{M}}_{\sigma}\Delta\hat{\mathbf{d}}=\int_A \delta\hat{\mathbf{B}}^{\mathrm{T}}\hat{\mathbf{S}}^{\mathrm{T}}\hat{\boldsymbol{\sigma}}\mathrm{d}A$ and $\hat{\mathbf{E}}_{ep}$ is the elasto-plastic constitutive matrix.

MULTI-SCALE ANALYSIS PROCEDURE

Proposed multi-scale analysis is performed only in a critical part of the analysis domain, in which the beam and shell models overlap. In this region, we decompose the shell nodal displacement vector $\hat{\mathbf{d}}$ into a coarse-scale component and a difference term by using a decomposition matrix **N**, which is developed based on kinematic assumptions of the classical beam theory and projects the beam solution onto the nodal points of the shell model, i.e.

$$\delta\hat{\mathbf{d}}=\mathbf{N}\delta\bar{\mathbf{d}}+\delta\mathbf{d}' \tag{18}$$

in which the first and second terms on the right-hand side represent the variation of coarse-scale model and the difference, respectively. The **N** matrix can be written as

$$\mathbf{N}=\mathbf{YZ} \tag{19}$$

where the **Y** matrix includes cross-sectional coordinates and **Z** matrix is the interpolation matrix along the beam. The above decompositions of the displacement field (Eq. 18) can be used to decompose the strain vector of the shell model, i.e.

$$\delta\hat{\boldsymbol{\varepsilon}}=\hat{\mathbf{S}}\hat{\mathbf{B}}\left(\mathbf{N}\delta\bar{\mathbf{d}}+\delta\mathbf{d}'\right)=\delta\bar{\boldsymbol{\varepsilon}}+\delta\boldsymbol{\varepsilon}' \tag{20}$$

$$\delta\bar{\boldsymbol{\varepsilon}}=\hat{\mathbf{S}}\hat{\mathbf{B}}\mathbf{N}\delta\bar{\mathbf{d}} \tag{21}$$

$$\delta\boldsymbol{\varepsilon}'=\hat{\mathbf{S}}\hat{\mathbf{B}}\delta\mathbf{d}' \tag{22}$$

Similar to the strain, the stress vector of the local shell model can be decomposed. By substituting the above relations in, the shell equilibrium equation can be decomposed into two simultaneous equations, i.e.,

$$\delta\Pi_1=\delta\bar{\mathbf{d}}^{\mathrm{T}}\mathbf{N}^{\mathrm{T}}\int_L\int_A \hat{\mathbf{B}}^{\mathrm{T}}\hat{\mathbf{S}}^{\mathrm{T}}\bar{\boldsymbol{\sigma}}\mathrm{d}A\mathrm{d}\bar{z}-\delta\bar{\mathbf{d}}^{\mathrm{T}}\mathbf{N}^{\mathrm{T}}\hat{\mathbf{f}}+\delta\bar{\mathbf{d}}^{\mathrm{T}}\mathbf{F}=0 \tag{23}$$

$$\delta\Pi_2=\delta\mathbf{d}'^{\mathbf{T}}\int_L\int_A \hat{\mathbf{B}}^{\mathrm{T}}\hat{\mathbf{S}}^{\mathrm{T}}\hat{\boldsymbol{\sigma}}\mathrm{d}A\mathrm{d}\bar{z}-\delta\mathbf{d}'^{\mathbf{T}}\hat{\mathbf{f}}=0 \tag{24}$$

The latter two equations are linearised to form a basis for finite element formulation. The shell solution is obtained by imposing the displacement of the beam element as an interface boundary condition for the shell element. Consequently, the algorithm of the multiscale procedure can be summarised as follows. Firstly, the global beam model is solved to obtain the initial displacement field while the local shell model (fine-scale model) is fixed. Then the displacements obtained in the previous step are applied to the local shell model in its boundaries, and the local shell model is solved to obtain the local displacement values. Two criteria are checked in each step within the framework of multiscale method. First criterion is to satisfy that the global equilibrium is achieved while the second criterion requires the vanishing of difference stress vector between the beam and the shell model to ensure that the two solutions are synchronised. Until the second criterion is satisfied, the difference stress vector is applied to the model as a complementary force until this force becomes smaller than a predefined tolerance.

VERIFICATION OF THE SHELL ANALYSIS

Before using multi-scale developments in the present model, the elasto-plastic shell model implemented in Section 3 was verified. Towards this goal, a cylinder panel under point load was considered. As shown in Figure 4.a, the curve edge nodes of the panel are assumed to be free in all directions while the side nodes are fixed against translation in all three directions. The modulus of elasticity, the Poisson ratio and the yield stress is taken

as 3.103kN/mm2, 0.3, and .001kN/mm2, respectively. The results are obtained by using 20x10 elements, i.e., 20 elements along the curved direction and 10 elements along the fixed edge direction, and compared with those obtained by the TRIC continuum formulation of Argyris et al. (2002) as shown in Figure 4.b and excellent agreement is observed.

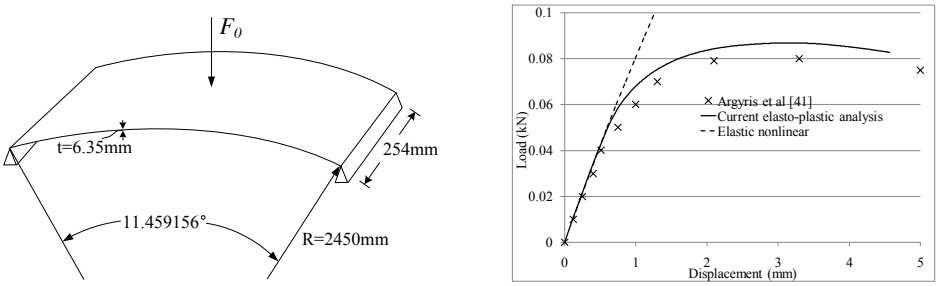

(a) Dimensions and loading (b) Load-deflection relations in the middle

Figure 4 Description of the arch and load-deflection relations

NUMERICAL EXAMPLES

As shown in **Figure 5**.a, the pipe analysed has a 17.15m span, a 1m diameter and a 25mm wall thickness. The pipe is fixed at the bottom end and is subject to a compressive force up to 15000 kN acting at the top and a total lateral load up to 15 kN (F_y=*7.5* kN).

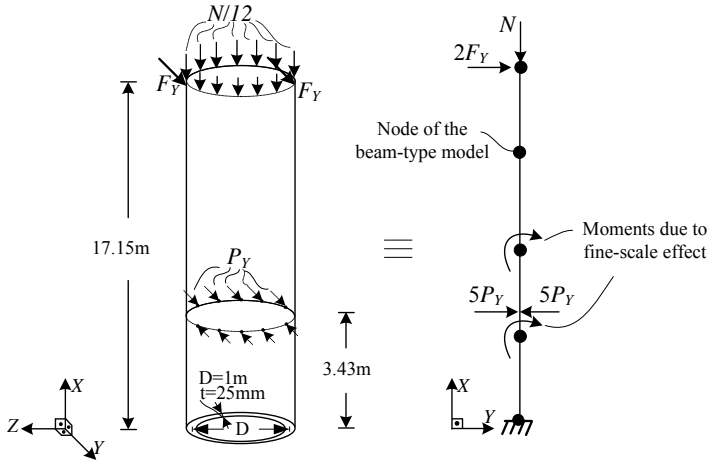

(a) Dimensions and loading of the pipe in the shell model (b) Equivalent multi-scale model

Figure 5 Description of the modelling of the pipe

The pipe is pinched at height *z=3430mm* through two equal and opposite sets of five forces 5Py as shown in **Figure 5** (up to a value of P_y=*1800* kN), such that it induces distortion within the cross-section as well as plastic deformations. Modulus of elasticity and the Poisson's ratio used in this example *E=300* GPA and *v=0.3*, respectively. The yield stress was taken as 300MPa and no hardening was assumed.

For the beam-type and multi-scale analyses four equal-span elements are used. In the shell analysis, the circumference was divided into 12 shell elements and the pipe height was sub-divided into 30 elements. The axial load is applied as distributed load acting at the nodes of the top cross-section of the shell model. In the multi-scale analysis, the cross-section is again divided into 12 shell elements and span was sub-divided into 14 elements. In order to verify the validity of the beam-type analyses, we also present a comparison against the constrained shell solution which is obtained by applying multiple-point constraints on the nodal displacements of the shell model based on the decomposition matrix **N** and adopting the beam constitutive matrix **E**.

Firstly, a linearly elastic analysis was conducted. The applied loads were a compressive force (i.e., *N=15000* kN) and a small lateral force, (F_y=*7.5* kN). The load versus tip horizontal deflection and tip rotation curves are plotted as shown in Figure 6.a, and b respectively.

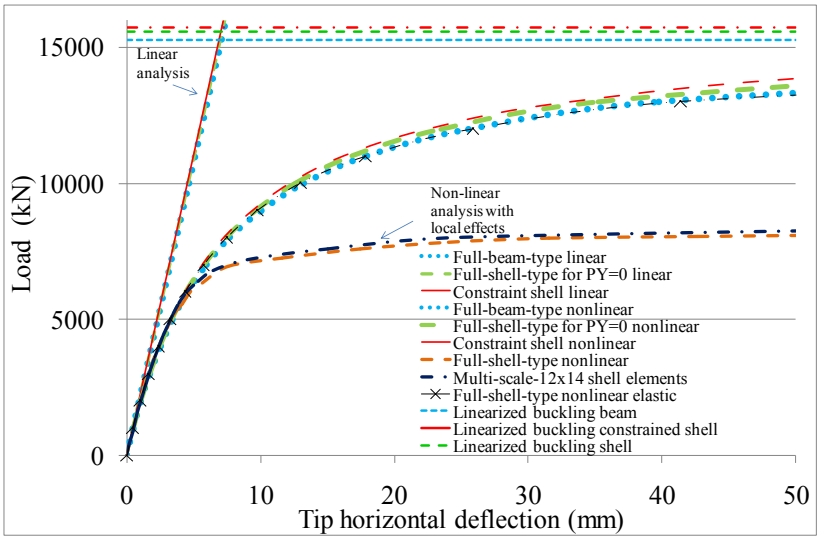

Figure 6 Description of the arch and load-deflection relations

Secondly, buckling loads based on a linearized buckling analysis corresponding to beam-type, constraint-shell-type and full-shell-type analysis are found as P_A=715,277kN, P_A=15,740kN and P_A=15,587kN, respectively, thus verifying the validity of beam analysis model, and suggesting that ovalization in this case have a negligible effect on the results. In the shell analysis, it was verified that no plastic deformations have taken place.

Thirdly, a nonlinear analysis was conducted, in which the loads were incremented from N=0, F_y=0 to a maximum of N=*15000* kN, F_y=*7.5* kN without pinching loads (i.e., P_Y=0). As shown in Figure 6.a-b, excellent agreement is observed between the beam analysis and the shell analysis.

Fourthly, in addition to the applied compressive loads, pinching loads were incrementally applied from zero to P_Y=*1800* kN in order to induce additional distortional deformations as well as plastic deformation. The corresponding load versus deflection curves are also shown in Figure 6.a and b. It should be noted that the comparison with fully elastic solution under local loads shows that plastic deformations are attained. The load versus deflection curves for the constrained shell and beam-type solutions are observed to be identical to those of the case where P_Y=0. On the other hand, when local deformations are introduced, the plastic deformations cause softening effect and increase the overall deflections of the full shell-type solution, which are not captured using the beam-type analysis given the rigid cross-section and elastic material response assumptions. In contrast, the multi-scale solution is very efficient in capturing the same behaviour as that predicted by the full shell-type analysis. In the multi-scale analysis, an overlapping region was considered between z=*0* and z=8003.33mm. The results are in very good agreement as can be verified from Figure 6.

CONCLUSIONS

In this paper, an analysis method based on the multi-scale domain decomposition approach was developed for the elasto-plastic analysis of pipes. The multi-scale domain decomposition allows the method to incorporate the effects of local deformations on the overall behaviour of the pipe by using a shell model only within the region of local deformations. A pipe buckling case was analysed and the results of the multi-scale analysis procedure proposed herein were compared with those of the full shell- and beam-type analyses. It was shown that very accurate results are obtained using the proposed analysis procedure.

REFERENCES

Argyris, J. H., Papadrakakis, M., & Karapitta, L. (2002). Elasto-plastic analysis of shells with the triangular element TRIC. *Computer Methods in Applied Mechanics and Engineering, 191*(33), 3613-3636.

Babuška, I., Banerjee, U., & Osborn, J. E. (2003). Survey of meshless and generalized finite element methods: A unified approach. *Acta Numerica, 12*, 1-125.

Babuška, I., & Melenk, J. M. (1997). The partition of unity method. *International Journal for Numerical Methods in Engineering, 40*(4), 727-758.

Bathe, K. J., & Almeida, C. A. (1982). SIMPLE AND EFFECTIVE PIPE ELBOW ELEMENT - INTERACTION EFFECTS. *Journal of Applied Mechanics, Transactions ASME, 49*(1), 165-171.

Belytschko, T., Krongauz, Y., Organ, D., Fleming, M., & Krysl, P. (1996). Meshless methods: An overview and recent developments. *Computer Methods in Applied Mechanics and Engineering, 139*(1-4), 3-47.

Belytschko, T., Moës, N., Usui, S., & Parimi, C. (2001). Arbitrary discontinuities in finite elements. *International Journal for Numerical Methods in Engineering, 50*(4), 993-1013.

Cook, R. D. (1990). Simulating curved elements by offsets. Rationale and application to shells of revolution. *Engineering computations, 7*(1), 79-80.

Cook, R. D., Malkus, D. S., Plesha, M. E., & Witt, R. J. (2002). *Concepts and applications of finite element analysis* (fourth ed.): John Wiley & Sons.

Crisfield, M. A. (1991). *Non-linear finite element analysis of solids and structures* (Vol. 1). New York: Wiley.

Erkmen, E., & Bradford, M. A. (2011). Coupling of finite element and meshfree methods be for locking-free analysis of shear-deformable beams and plates. *Engineering Computations (Swansea, Wales), 28*(8), 1003-1027.

Erkmen, R. E. (2013). Bridging multi-scale approach to consider the effects of local deformations in the analysis of thin-walled members. *Computational Mechanics, 52*(1), 65-79.

Haidar, K., Dubé, J. F., & Pijaudier-Cabot, G. (2003). Modelling crack propagation in concrete structures with a two scale approach. *International Journal for Numerical and Analytical Methods in Geomechanics, 27*(13), 1187-1205.

Hobbs, R. E. (1981). Pipeline buckling caused by axial loads. *Journal of Constructional Steel Research, 1*(2), 2-10.

Houliara, S., & Karamanos, S. A. (2006). Buckling and post-buckling of long pressurized elastic thin-walled tubes under in-plane bending. *International Journal of Non-Linear Mechanics, 41*(4), 491-511.

Houliara, S., & Karamanos, S. A. (2010). Stability of long transversely-isotropic elastic cylindrical shells under bending. *International Journal of Solids and Structures, 47*(1), 10-24.

Hughes, T. J. R., & Sangalli, G. (2007). Variational multiscale analysis: The fine-scale green's function, projection, optimization, localization, and stabilized methods. *SIAM Journal on Numerical Analysis, 45*(2), 539-557.

Ibrahimbegovic, A., Taylor, R. L., & Wilson, E. L. (1990). Robust quadrilateral membrane finite element with drilling degrees of freedom. *International Journal for Numerical Methods in Engineering, 30*(3), 445-457.

Ju, G. T., & Kyriakides, S. (1992). Bifurcation and localization instabilities in cylindrical shells under bending-II. Predictions. *International Journal of Solids and Structures, 29*(9), 1143-1171.

Karamanos, S. A. (2002). Bending instabilities of elastic tubes. *International Journal of Solids and Structures, 39*(8), 2059-2085.

Karamanos, S. A., & Tassoulas, J. L. (1996). Tubular members. I: Stability analysis and preliminary results. *Journal of Engineering Mechanics, 122*(1), 64-71.

Li, S., & Liu, W. K. (2002). Meshfree and particle methods and their applications. *Applied Mechanics Reviews, 55*(1), 1-34.

Liu, W. K., Hao, S., Belytschko, T., Li, S., & Chang, C. T. (2000). Multi-scale methods. *International Journal for Numerical Methods in Engineering, 47*(7), 1343-1361.

Liu, W. K., Park, H. S., Qian, D., Karpov, E. G., Kadowaki, H., & Wagner, G. J. (2006). Bridging scale methods for nanomechanics and materials. *Computer Methods in Applied Mechanics and Engineering, 195*(13-16), 1407-1421.

Liu, W. K., Uras, R. A., & Chen, Y. (1997). Enrichment of the finite element method with the reproducing kernel particle method. *Journal of Applied Mechanics, Transactions ASME, 64*(4), 861-870.

Militello, C., & Huespe, A. E. (1988). A displacement-based pipe elbow element. *Computers and Structures, 29*(2), 339-343.

Mosler, J. (2005). On the efficient implementation of an elastoplastic damage model for large-scale analyses of material failure: a multiscale approach. *Computers & Structures, 83*(4–5), 369-382.

Nowzartash, F., & Mohareb, M. (2004). An elasto-plastic finite element for steel pipelines. *International Journal of Pressure Vessels and Piping, 81*(12), 919-930.

Ozkan, I. F., & Mohareb, M. (2009). Testing and analysis of steel pipes under bending, tension, and internal pressure. *Journal of Structural Engineering, 135*(2), 187-197.

Qian, D., Wagner, G. J., & Liu, W. K. (2004). A Multi-scale projection method for the analysis of carbon nanotubes. *Computer Methods in Applied Mechanics and Engineering Computations (Swansea, Wales), 193*, 1603-1632.

Song, H.-W., & Tassoulas, J. L. (1993). Finite element analysis of propagating buckles. *International Journal for Numerical Methods in Engineering, 36*(20), 3529-3552.

Wagner, G. J., & Liu, W. K. (2003). Coupling of atomistic and continuum simulations using a bridging scale decomposition. *Journal of Computational Physics, 190*(1), 249-274.
Weicker, K., Salahifar, R., & Mohareb, M. (2010). Shell analysis of thin-walled pipes. Part II - Finite element formulation. *International Journal of Pressure Vessels and Piping, 87*(7), 414-423.